

# $\gamma'$ Phase Stability and Phase Equilibrium in Ternary Co-Al-W at 900 °C

Eric A. Lass, Maureen E. Williams, Carelyn E. Campbell, Kil-Won Moon, and Ursula R. Kattner

(Submitted July 16, 2014; in revised form September 5, 2014; published online October 15, 2014)

Phase equilibria at 900 °C in the Co-rich Co-Al-W ternary system are investigated through isothermal annealing of six alloy compositions for times up to 8000 h. The volume fraction of the L1<sub>2</sub>- $\gamma'$  phase co-existing with disordered FCC- $\gamma$ , B2 and D0<sub>19</sub> phases is found to steadily decrease with increasing annealing time indicating that it is unstable at 900 °C. Additional heat treatments at 850 and 1000 °C further suggest it is a nonequilibrium phase at all temperatures in the ternary system. The L1<sub>2</sub>- $\gamma'$  phase dissolves slowly with significant amounts remaining in some alloys after 8000 h at 900 °C. However, the present work clearly indicates the microstructure is moving toward a three-phase equilibrium between  $\gamma$ , D0<sub>19</sub>, and B2. The collected compositional and phase equilibria information provide much needed data for improving the available thermodynamic assessments of the ternary Co-Al-W alloy system.

**Keywords** Co-based, phase diagram, phase equilibrium, superalloy, thermodynamics

## 1. Introduction

High temperature Ni-based superalloys owe their excellent high temperature strength and creep resistance properties to their microstructure consisting of a high volume fraction of coherent ordered L1<sub>2</sub>- $\gamma'$  precipitates in a disordered FCC- $\gamma$  matrix. Since the discovery of an analogous  $\gamma$ - $\gamma'$  two-phase region in ternary Co-Al-W alloys,<sup>[1]</sup> significant research interest has been focused on the system. Alloys containing a relatively low number of elements (three to five), compared to mature Ni-based alloys containing as many as ten or more elements, have demonstrated promising elevated temperature properties;<sup>[2]</sup> while the higher melting temperature of Co compared to Ni creates the possibility of increased operating temperatures, and in turn, improved efficiency of turbine applications for which they are used.

Despite major efforts to exploit the potential of Co-based  $\gamma$ - $\gamma'$  alloys, the thermodynamics and phase equilibria in the base ternary system, Co-Al-W, have largely been neglected. In their original publication in 2006, Sato et al. presented preliminary isothermal sections of the Co-rich portion of the phase diagram at 900 and 1000 °C.<sup>[1]</sup> Since then, very little work has been published regarding phase equilibria in Co-Al-W; and the work that has been published is

contradictory. Dmitrieva et al.<sup>[3]</sup> studied the liquidus and solidus surfaces in the Co-rich corner and presented two vertical sections of the phase diagram, one for a mole fraction of Co of 75 % and the other for equiatomic Al and W content, but no mention of the ordered  $\gamma'$  phase was made. Kobayashi et al.<sup>[4]</sup> studied phase equilibria in the ternary system at 900 °C for annealing times up to 2000 h using a diffusion couple technique, concluding that the  $\gamma'$  phase was metastable. This result was supported by the work of Tsukamoto et al. on a bulk cast alloy.<sup>[5]</sup> More recently, Xue et al. studied the microstructure of several compositions after annealing at 900 °C for up to 1000 h, concluding that  $\gamma'$  is an equilibrium phase.<sup>[6]</sup>

Because of the contradictory results regarding phase equilibria in ternary Co-Al-W, most work in this system either assumes that the  $\gamma'$  phase is an equilibrium one or ignores the question entirely, noting that additional alloying elements will be required to further stabilize the  $\gamma'$  phase anyway. Several recent Calphad thermodynamic assessments have been performed assuming  $\gamma'$  is an equilibrium phase at 900 °C.<sup>[2,7–9]</sup> Other work has focused on the mechanical properties of ternary and higher order alloys,<sup>[10–17]</sup> the evolution and coarsening behavior of two-phase  $\gamma$ - $\gamma'$  microstructure,<sup>[13,15,18–20]</sup> or the microstructure and partitioning behavior of quaternary and higher order alloying elements.<sup>[13,15,21–25]</sup> Furthermore, the only experimental data available for temperatures other than 900 °C are the 1000 °C isothermal section presented by Sato et al.<sup>[1]</sup> and data reported by Xue et al. at 1300 °C.<sup>[6]</sup>

If the development of new high temperature alloys based on the Co-Al-W ternary system is to be realized, an accurate understanding of the thermodynamics and phase equilibria of the system is essential as the foundation for building useful thermodynamic databases for alloy design and discovery. The purpose of this work is to answer some of the outstanding questions with respect to the ternary Co-Al-W system, and to gather the required phase equilibria data for constructing such a database. The focus of the present study is the 900 °C isothermal section. However some

Eric A. Lass, Maureen E. Williams, Carelyn E. Campbell, Kil-Won Moon, and Ursula R. Kattner, Materials Science & Engineering Division, National Institute of Standards and Technology, 100 Bureau Dr., M/S 8555, Gaithersburg, MD 20899, USA. Contact e-mail: eric.lass@nist.gov.

results are presented at different temperatures, and will be the subject of future work.

## 2. Experimental Methods

The six alloys investigated in the present study are plotted on the phase diagram in Fig. 1, which was redrawn from the diagram of Kobayashi et al., in which they included as dashed lines the proposed regions of three-phase metastable equilibrium between  $\gamma'$  and the three surrounding phases  $\gamma$ ,  $DO_{19}$ , and  $B2$ .<sup>[4]</sup> The compositions of the investigated alloys consist of a binary Co-W alloy, one alloy contained within each of the three three-phase regions surrounding the  $\gamma'$  single phase field, and two alloys near or within the two-phase  $\gamma$ - $\gamma'$  field, one where the  $\gamma$  phase should be the majority phase at equilibrium and one with the  $\gamma'$  phase as the majority phase. The nominal compositions for all the alloys are given in Table 1 (by mole fraction), along with the measured compositions of the as-prepared alloys.

The alloys were prepared by weighing the appropriate amounts of pure Al (mass fraction of 99.99 %), Co (mass fraction of 99.98 %), and W (mass fraction of 99.9 %) sufficient to produce a 30 g ingot; then arc melting under an inert Ar atmosphere. Al evaporation loss was minimized by first melting together the Co and W to reduce the alloy melting temperature and to ensure complete melting of W prior to Al addition. Despite this procedure, experience

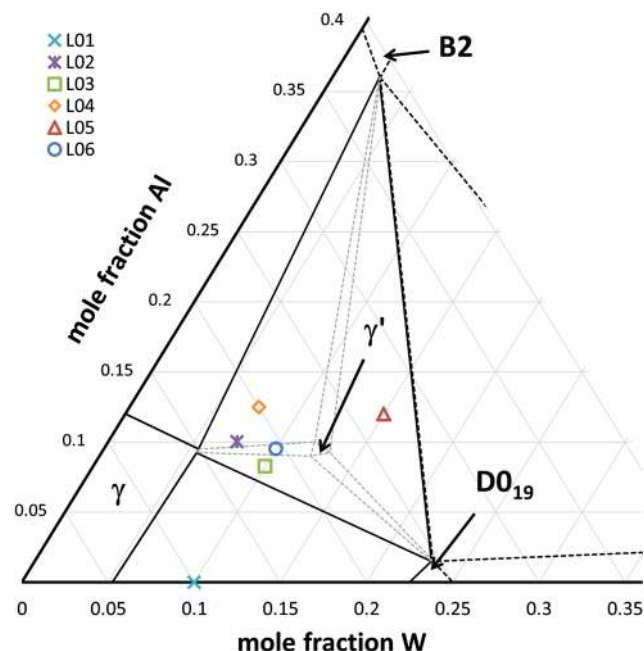


**Fig. 1** The ternary Co-Al-W phase diagram redrawn from Kobayashi et al.<sup>[4,5]</sup> where the  $\gamma'$  phase and accompanying two-phase regions are shown as dotted lines to signify the metastability of the  $\gamma'$  phase. The six alloy compositions in the present study are shown

**Table 1** The target and measured compositions (in mole fraction) of the six as-spun alloy ribbons investigated in the present study

Alloy designation	Target composition		Measured composition	
	Al, %	W, %	Al, %	W, %
L01	...	10	...	10.27 ± 0.25
L02	10	7.5	9.98 ± 0.57	7.58 ± 0.29
L03	8.25	10	8.29 ± 0.53	10.10 ± 0.22
L04	12.5	7.5	12.41 ± 0.55	7.65 ± 0.26
L05	12	15	12.17 ± 0.54	13.98 ± 0.28
L06	9.5	10	9.49 ± 0.52	10.13 ± 0.24

The uncertainties represent 95 % confidence intervals

demanding that an additional fraction of 2.5 % of the required mass of Al be added to the measured charge to compensate for Al evaporation during the melting process. The samples were flipped and remelted 5-6 times.

The as-cast ingots were then cut into 1-2 g pieces and melt-spun (MS) using a ZrO<sub>2</sub>-coated quartz crucible onto a rotating Cu wheel spinning at 1000 RPM under a He atmosphere. The resulting ribbons were 1-3 mm in width, a few centimeters in length, and between 30 and 80  $\mu$ m thick. The ribbon material was then encapsulated in quartz ampules under an inert He atmosphere and annealed at a temperature of 900 °C for up to 8000 h; followed by a room temperature brine quench. The as-spun and annealed ribbons were characterized using x-ray diffraction (XRD) and scanning electron microscopy (SEM) equipped with a back-scatter electron (BSE) detector and energy dispersive x-ray spectrometer (EDS). Pure elemental Al, Co, and W, of the purity describe above, were used as standards for EDS analysis. The extremely fine microstructure of the as-spun ribbons permitted use of the EDS to determine the bulk compositions and provided an ideal nearly homogeneous starting material for subsequent heat treatment. The uncertainty in the measured compositions was expressed as twice the calculated standard deviation of the measurements, or approximately a 95 % confidence level; where the total standard deviation was determined from both that reported for the EDS instrument and that arising from the repeatability of at least five measurements. The chosen EDS spectrum acquisition parameters yielded instrument standard deviations of 0.10, 0.28, and 0.24 % (mole fraction), for Al, Co, and W, respectively.

The volume fractions of phases present in the alloys after the various heat treatments were estimated via image analysis of multiple representative microstructures using the difference in shading between the various phases in the BSE images. As an example, consider a microstructure containing  $\gamma$ ,  $\gamma'$ ,  $DO_{19}$  and  $B2$  (Fig. 3d). The  $\gamma$  and  $\gamma'$  phases may occur either as part of a two-phase microconstituent (light + dark gray  $\gamma + \gamma'$  regions in Fig. 3d) or as larger coarsened particles (dark gray  $\gamma$  in Fig. 3d). To properly quantify the amounts of all four phases, and for both

possible regions of existence of  $\gamma/\gamma'$ , the images were analyzed in the following way. First, using low magnification images representative of the entire sample structure, the fraction of pixels corresponding to the white  $D0_{19}$  and black B2 phases were counted. Second, the fraction of pixels belonging to both the B2 phase and the dark gray coarsened  $\gamma$  phase was determined; and the fraction of B2 determined above was subtracted to yield the amount of coarsened  $\gamma$ . In the lower magnification images, the  $\gamma + \gamma'$  regions were typically too fine to resolve the individual phases and it could be treated as a separate grey-scale phase for image analysis purposes. Thus the  $\gamma$  contained within it was, for the most part, not counted during this step. The total fraction of the two-phase  $\gamma + \gamma'$  microconstituent was then determined by subtracting the pixels identified as  $D0_{19}$ , B2, or coarsened  $\gamma$ , from the total pixels in the image. Finally, the fractions of  $\gamma$  and  $\gamma'$  within the two-phase region were determined by analyzing images of only the two-phase structure at high magnification. The analysis software was used as much as possible to process the images and distinguish between phases to avoid human subjectivity; however it was necessary to provide some input to determine the cutoff points between the shading of each phase. Several systematic analyses of single images revealed a standard deviation in the volume fraction of 1.9 % from the mean calculated volume fraction of a given phase. This number was used along with the standard deviation of several repeated measurements to determine the uncertainty of the volume fraction measurements, expressed again as twice the combined standard deviation, or a 95 % confidence level.

### 3. Results and Discussion

#### 3.1 As-spun Microstructure

Figure 2 presents BSE micrographs of the as-spun microstructures for the six alloy ribbons. Four of the alloys, 10 W<sup>1</sup> (L01), 10Al-7.5W (L02), 8.25Al-10W (L03), and 9.5Al-10W (L06) appear to be single phase FCC- $\gamma$  as determined by via XRD (not shown). The microstructure of the 7.5W-12.5Al (L04) composition is primarily single phase FCC- $\gamma$  with small B2 (CoAl) particles at grain boundaries (GBs); while the 12Al-15W (L05) alloy contains both B2 and  $\mu$  phases (Co<sub>7</sub>W<sub>6</sub>-D8<sub>5</sub>) along the GBs. The secondary phase precipitates in both L04 and L05 are on the order of 100 nm in size; and the  $\mu$  observed in the as-spun L05 is found to completely dissolve after 1000 h at 900 °C. The FCC grain size of all six alloys is fairly uniform with an average size between 5 and 15  $\mu$ m. TEM investigation of the as-spun materials showed varying degrees of L1<sub>2</sub> ordering within the FCC phase of each alloy, appearing as clusters on the order of 2-5 nm within the FCC matrix. This

result is consistent with the observations of Meher et al. in solutionized and quenched bulk alloys.<sup>[20]</sup>

#### 3.2 Microstructural Evolution and $\gamma'$ Stability

**3.2.1 Behavior at 900 °C.** The microstructures of the alloys obtained in the present study, located within the three-phase fields at 900 °C originally proposed by Sato et al. (Fig. 1), are shown in Fig. 3 to 5 for annealing times between 168 and 8000 h. After 168 h (Fig. 3a) the majority of the L03 microstructure consists of the  $\gamma + \gamma'$  cuboidal microconstituent; as well as larger regions of coarse  $D0_{19}$  (white) and  $\gamma$  (dark gray). After 1000 h (Fig. 3b), the fraction of  $\gamma + \gamma'$  decreases, while the amount of coarsened  $\gamma$  (dark gray) and  $D0_{19}$  (white) increases. Regions of coarsened  $\gamma'$  (light gray) are also observed. Both Fig. 3(a) and (b) support the original Sato phase diagram and the results reported by Xue et al. However, after further annealing of L03 for times of 2000 h and beyond, Fig. 3(c)-(e), a fourth phase, B2 (black), precipitates out and begins to grow, contradictory to these previous results.

Annealing of alloys L04 and L05 reveal 4-phase microstructures for all annealing times: Fig. 4 for alloy L04 and Fig. 5 for L05. These results are also inconsistent with the original diagram and the findings of Xue et al. for a heat treatment at 900 °C and for 1000 h:  $D0_{19}$  should not be present in alloy L04 and  $\gamma$  should not be present in alloy L05. Clearly equilibrium has not been reached even after 8000 h because, according to the Gibbs phase rule, four phases cannot be in equilibrium in a ternary system except at special temperatures. In L03, the B2 phase emerges after a heat treatment for 2000 h at 900 °C; while the amount of the  $D0_{19}$  phase in L04 is observed to increase. As the B2 and  $D0_{19}$  phases form and become more prevalent with increasing annealing time, the fraction of  $\gamma'$  decreases. Figure 6 presents the volume fraction of each phase as a function of annealing time for each of the five ternary alloys in the present study.

Microstructural evolution in L06, although not shown here, is very similar to that of L03, except the microstructure contains a higher volume fraction of  $\gamma'$  for the same annealing time compared to alloy L03. Yet, from Fig. 6(e), the amount of  $\gamma'$  also decreases with increasing heat treatment time; and B2 is observed to form after annealing for 4000 h at 900 °C. The L06 sample annealed at 900 °C for 8000 h was lost because the quartz ampule was broken during the heat treatment. The microstructural evolution of L02 on the other hand behaves much like L04 (Fig. 6a). The L02 samples annealed for 4000 h and 8000 h at 900 °C exhibited appreciable loss in Al content compared to the nominal compositions. The likely cause of the loss of Al is its evaporation from the ribbon surface. All five ternary ribbon compositions showed signs of some Al loss up to about 10  $\mu$ m from the ribbon surfaces. However the total ribbon thickness for these compositions exceeded 50  $\mu$ m, leaving at least 30  $\mu$ m in the ribbon center with a composition nearly equal to the nominal bulk compositions (see Table 2). The L02 ribbons annealed for 4000 and 8000 h were found to be only about 20  $\mu$ m, causing the entire sample to exhibit Al loss. As a result, bulk compositions of L02 annealed at 4000

<sup>1</sup>The alloy compositions throughout the text are designation by mole fraction of W and Al. For instance, an alloy described as 7.5W-10Al contains a mole fraction of W of 7.5 %, a mole fraction of 10 % Al, and a balance of Co.

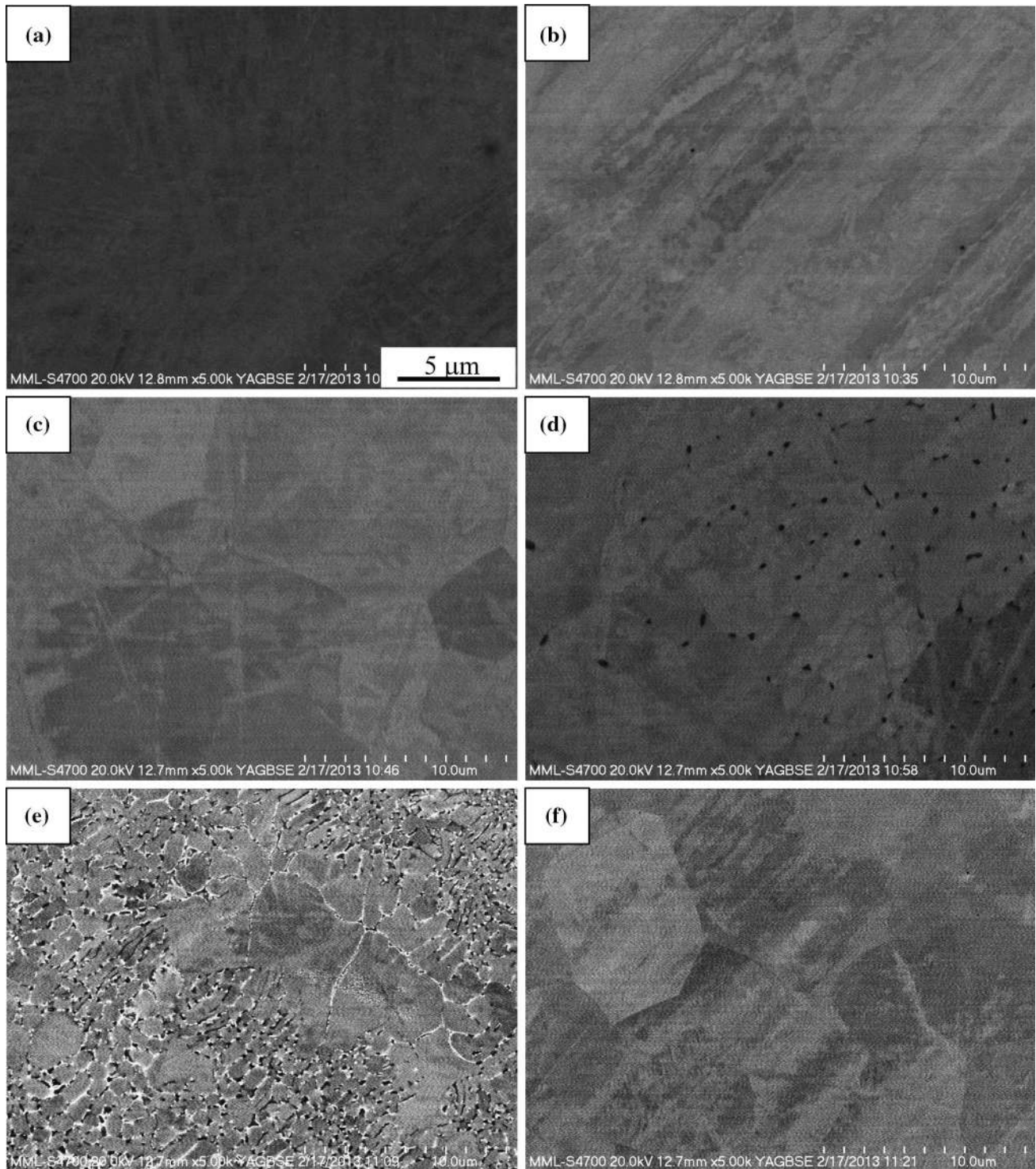


**Fig. 2** BSE micrographs of the as-spun ribbons: (a) L01 (Co-10W), (b) L02 (Co-10Al-7.5W), (c) L03 (Co-8.25Al-10W), (d) L04 (Co-12.5Al-7.5W), (e) L05 (Co-12Al-15W), and (f) L06 (Co-9.5Al-10W). Small precipitates of B2 (black) are found in (d) (L04); while both B2 and  $\mu$  (white) are found in the as-spun microstructure of L05 in (e). The scale bar in (a) is representative of all images (i.e. the magnifications are the same)

and 8000 h moved into the two phase  $\gamma + D0_{19}$  region of the phase diagram. These were the only two samples with compositions significantly different than alloy nominal

compositions. The bulk compositions of all other samples were found to deviate from the measured as-spun compositions by  $<0.5\%$ .

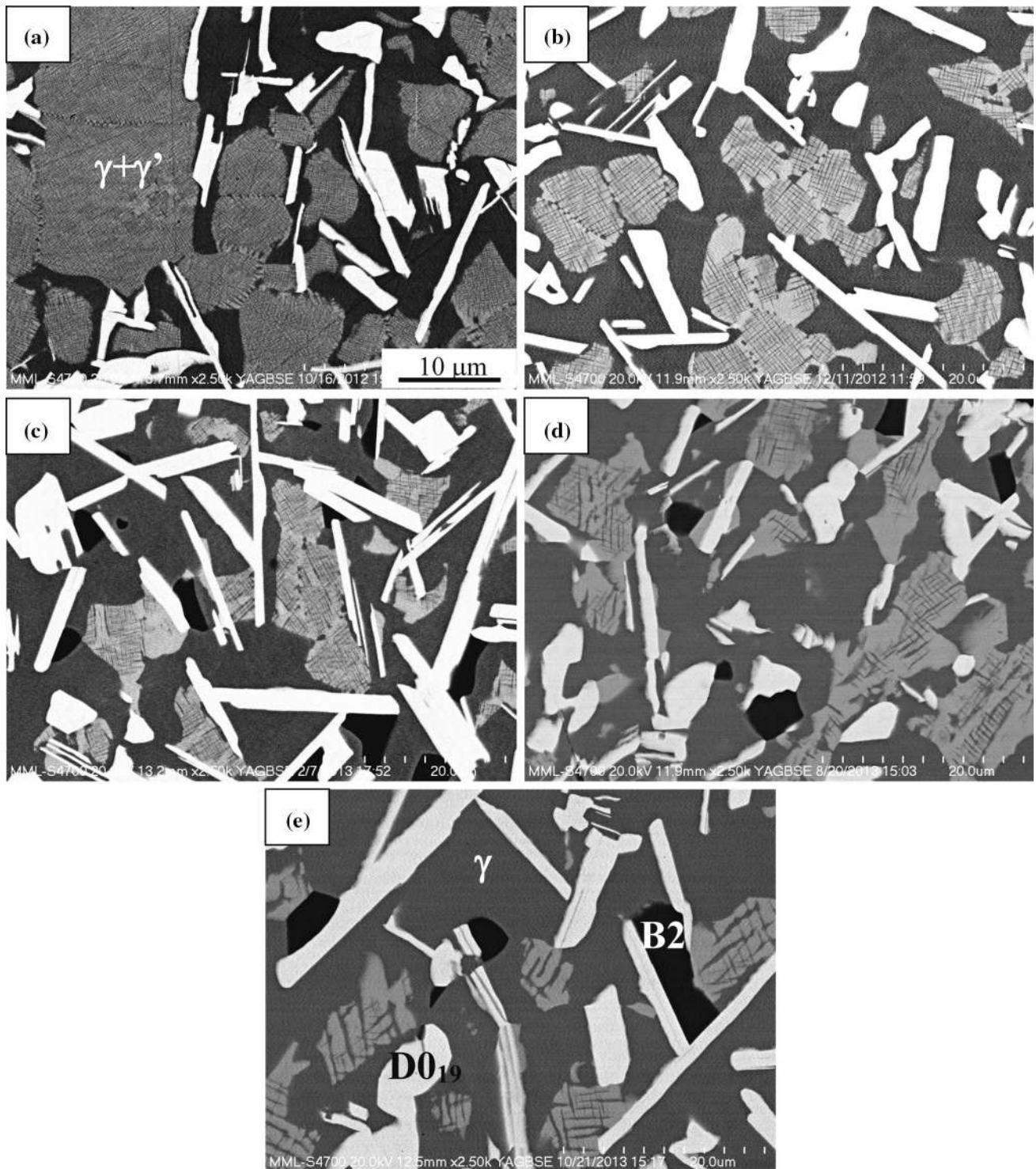


**Fig. 3** BSE micrographs of the L03 microstructure after annealing at 900 °C for (a) 168 h, (b) 1000 h, (c) 2000 h, (d) 4000 h, and (e) 8000 h. The brightest phase in each image is D0<sub>19</sub>, black is B2, dark gray is  $\gamma$ , and light gray is  $\gamma'$ . The scale bar in (a) is representative of all images (i.e. the magnifications are the same)

Despite the failure to reach equilibrium, the present study provides clear evidence of the instability of  $\gamma'$  in the ternary Co-Al-W system. According to the Gibbs phase rule, at constant pressure four phases can be in equilibrium with one

another only at specific points in composition and temperature space, e.g. a eutectic point. The appearance of a fourth phase in the alloys lying within the supposed three-phase regions would violate this fundamental thermodynamic rule;

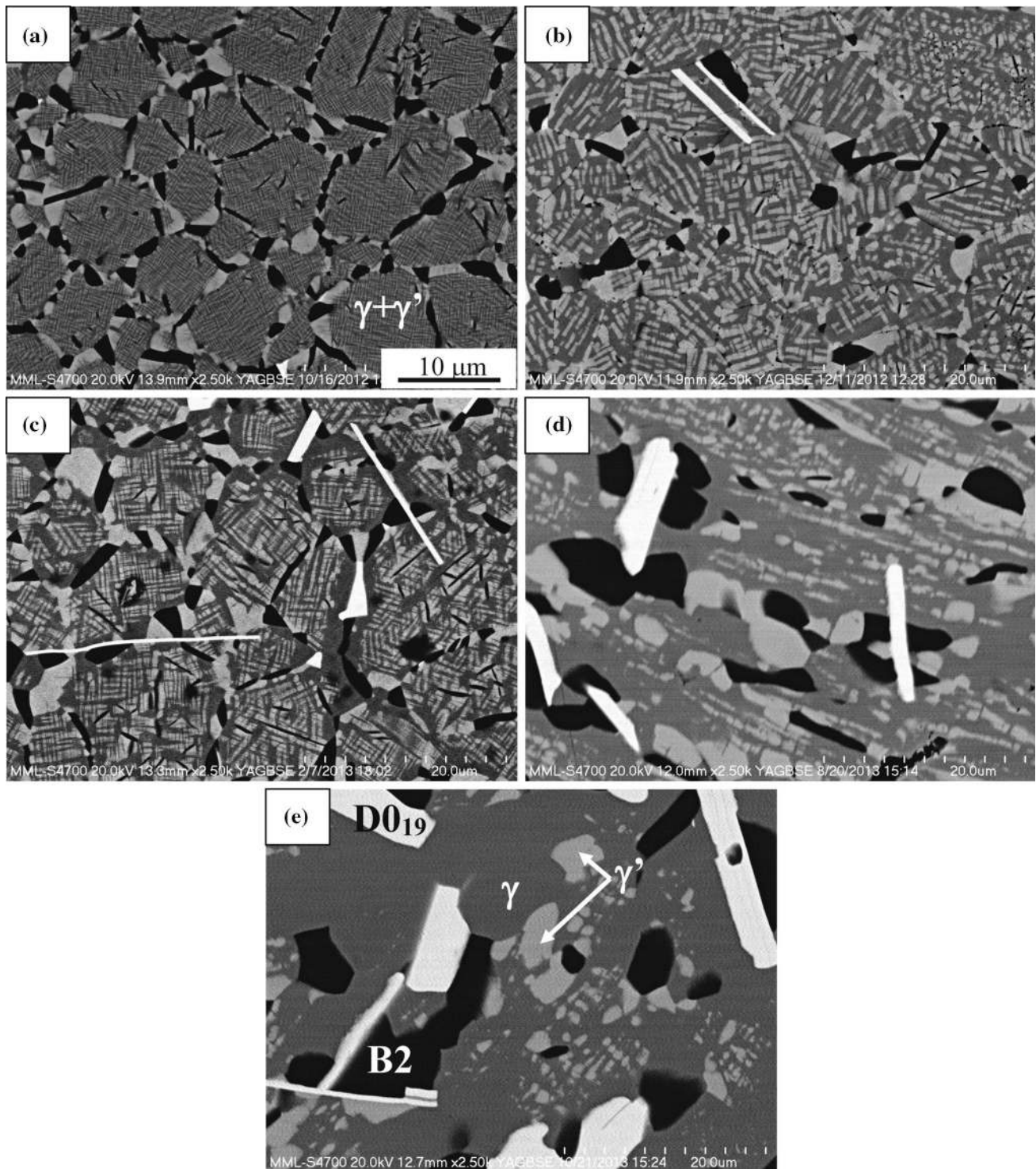


**Fig. 4** BSE micrographs of the L04 microstructure after annealing at 900 °C for (a) 168 h, (b) 1000 h, (c) 2000 h, (d) 4000 h, and (e) 8000 h. The brightest phase in each image is  $D0_{19}$ , black is B2, dark gray is  $\gamma$ , and light gray is  $\gamma'$ . The scale bar in (a) is representative of all images (i.e. the magnifications are the same)

i.e.  $D0_{19}$  in alloy L04 (selected to be in the three phase triangle  $\gamma + \gamma' + B2$ ), B2 in alloy L03 (selected to be in the three phase triangle  $\gamma + \gamma' + D0_{19}$ ),  $\gamma$  in L05 (selected to be in the three phase triangle  $\gamma' + B2 + D0_{19}$ ). When these

observations are combined with the observed decrease in the volume fraction of  $\gamma'$  and the increase in the volume fractions of  $D0_{19}$  and B2 with annealing time for all five ternary compositions, it can be concluded that  $\gamma'$  is the

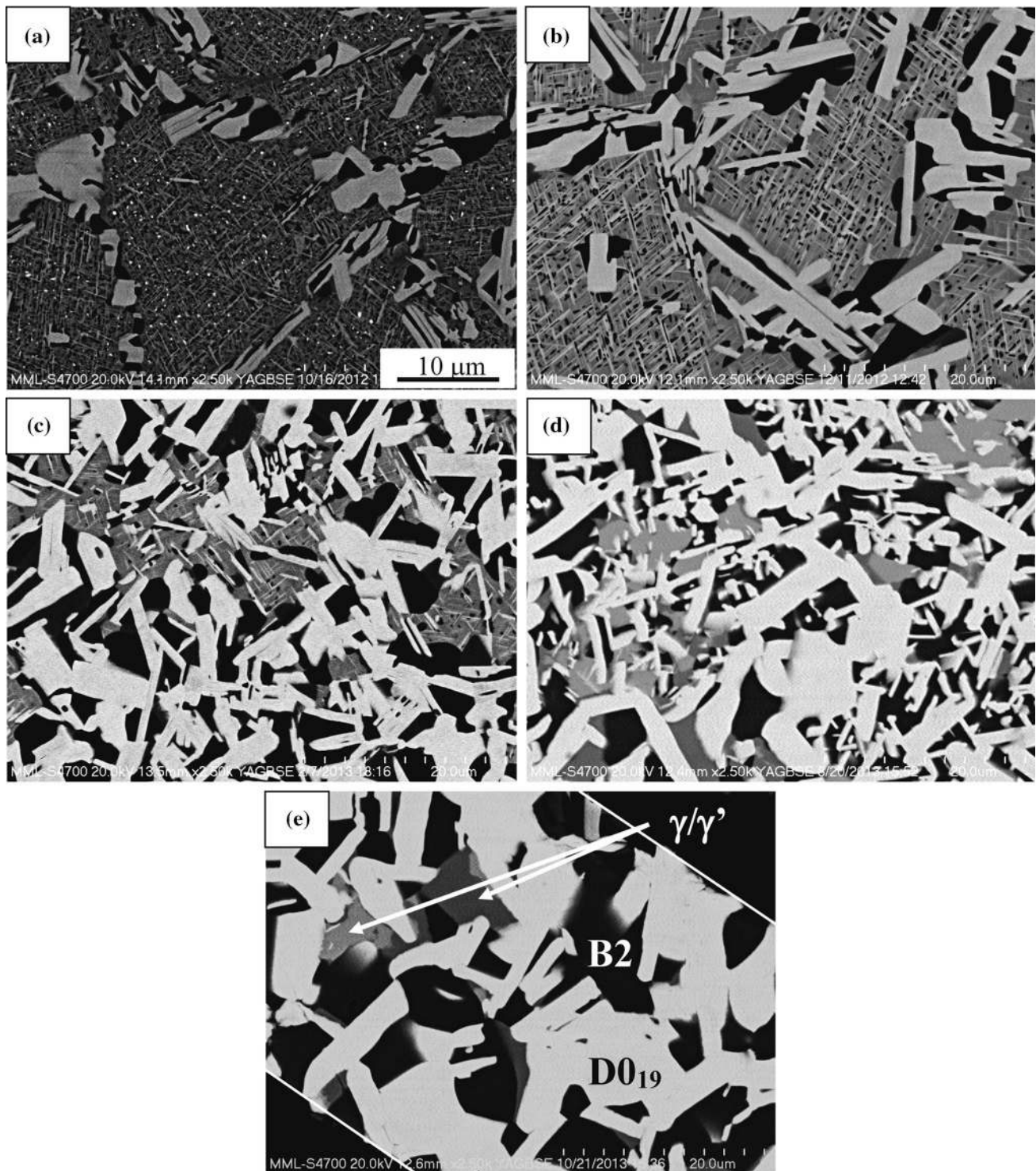


**Fig. 5** BSE micrographs of the L05 microstructure after annealing at 900 °C for (a) 168 h, (b) 1000 h, (c) 2000 h, (d) 4000 h, and (e) 8000 h. The brightest phase in each image is D0<sub>19</sub>, black is B2, dark gray is  $\gamma$ , and light gray is  $\gamma'$ . The fine specks of white in (a) are  $\mu$ -Co<sub>7</sub>W<sub>6</sub> formed during solidification. The thickness of the ribbon in (e) is narrow, and the dark upper-right and lower-left corners, indicated by the dashed lines, are beyond the edge of the ribbon, not B2. The scale bar in (a) is representative of all images (i.e. the magnifications are the same)

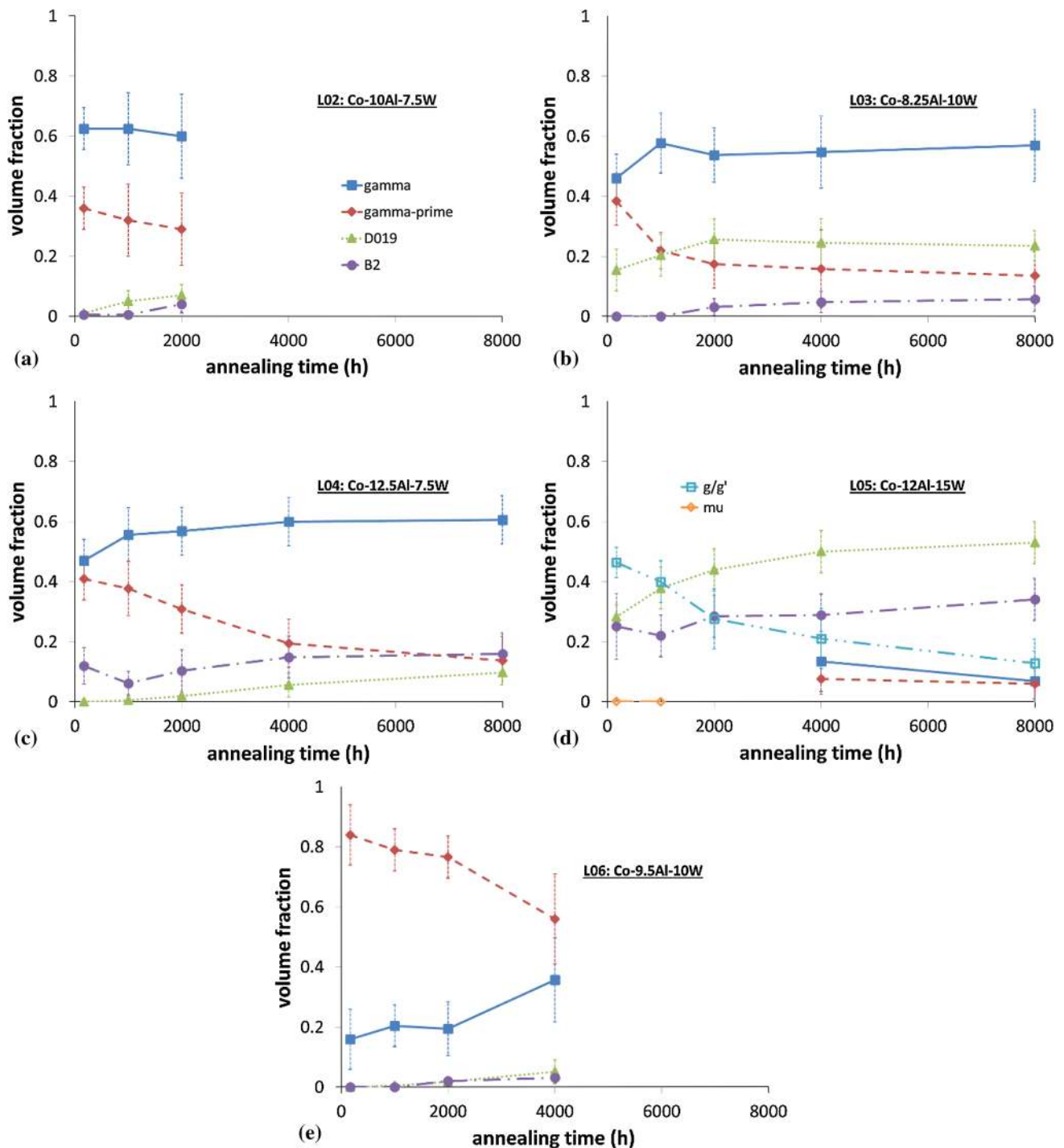


**Fig. 6** The volume fraction of each phase (measured as an area fraction from a micrograph) found in (a) L02, (b) L03, (c) L04, (d) L05, and (e) L06 as a function of annealing time at 900 °C. L02 samples annealed for 4000 and 8000 h of L06 samples annealed for 8000 h were not useable. In (d) the individual amounts of  $\gamma$  and  $\gamma'$  were not resolvable for times less than 4000 h due to the fine microstructure. The error bars represent 95 % confidence intervals

nonequilibrium phase; and all five evolving microstructures are moving toward a three-phase equilibrium of  $\gamma + D0_{19} + B2$  at 900 °C in this ternary system. Given enough time the  $L_{12}$ -phase will dissolve completely at 900 °C as suggested

in the phase diagram of Kobayashi et al. and Tsukamoto et al.<sup>[4,5]</sup>

**3.2.2 Stability of  $\gamma'$  at Other Temperatures.** Most of the available experimental work on ternary Co-Al-W has



**Table 2 Experimentally measured compositions (in mole fraction) of the bulk material and each phase found in the six ribbon compositions after annealing at 900 °C for 4000 h**

Alloy	Phase	Al, %	W, %
Kobayashi et al.	$\gamma$	9.4	5
	D0 <sub>19</sub>	1.7	22.9
	B2	37.4	2.7
This work: overall	$\gamma$	8.89 ± 0.83	5.64 ± 0.31
	D0 <sub>19</sub>	2.27 ± 0.58	21.65 ± 0.61
	B2	34.42 ± 1.33	2.96 ± 0.23
L01	$\gamma'$	9.38 ± 0.69	11.96 ± 0.20
	Bulk	...	9.86 ± 0.34
	$\gamma$	...	2.93 ± 0.55
L02	D0 <sub>19</sub>	...	23.45 ± 0.96
	Bulk	5.77 ± 0.58	8.03 ± 0.52
	$\gamma$	6.74 ± 0.88	5.65 ± 0.38
L03	D0 <sub>19</sub>	1.74 ± 0.68	21.86 ± 0.54
	Bulk	8.26 ± 1.22	9.84 ± 1.02
	$\gamma$	9.02 ± 0.55	5.53 ± 0.30
L04	D0 <sub>19</sub>	2.28 ± 0.55	21.56 ± 0.56
	B2	34.65 ± 0.98	2.90 ± 0.23
	$\gamma'$	9.58 ± 0.64	11.81 ± 0.41
L05	Bulk	12.47 ± 1.65	7.18 ± 0.59
	$\gamma$	9.17 ± 0.66	5.69 ± 0.30
	D0 <sub>19</sub>	2.31 ± 0.51	21.82 ± 0.56
L06	B2	34.65 ± 1.06	2.95 ± 0.22
	$\gamma'$	9.41 ± 0.62	12.03 ± 0.26
	Bulk	12.73 ± 1.59	13.96 ± 0.81
L05	$\gamma$	8.44 ± 0.60	5.90 ± 0.33
	D0 <sub>19</sub>	2.21 ± 0.58	22.41 ± 1.30
	B2	34.39 ± 2.33	3.22 ± 0.36
L06	$\gamma'$	9.10 ± 1.15	12.38 ± 0.92
	Bulk	9.05 ± 0.92	9.98 ± 0.92
	$\gamma$	8.56 ± 0.66	5.69 ± 0.23
L06	D0 <sub>19</sub>	2.21 ± 0.66	21.59 ± 0.67
	B2	33.41 ± 1.00	3.01 ± 0.22
	$\gamma'$	9.19 ± 0.61	12.03 ± 0.36

The overall compositions are averaged from the measurements on all alloys in the three-phase  $\gamma + D0_{19} + B2$  field. The uncertainties represent 95 % confidence intervals. No uncertainty was given by Kobayashi et al.<sup>[3]</sup>

been performed at 900 °C; and little is known of the phase equilibria at additional temperatures. Figure 7 presents the microstructural evolution of alloy L06 annealed at 850 and 1000 °C for two annealing times.

At 1000 °C, the alloy contains  $\gamma$  and  $\mu$  phases with very little  $\gamma'$  after 168 h (Fig. 7a); which further decreases to nearly zero after 1000 h (Fig. 7b). The microstructure looks to be moving toward an equilibrium  $\gamma + \mu$  two-phase field in agreement with Sato et al.<sup>[1]</sup> After 2000 h at 850 °C, shown in Fig. 7(c), just as at 900 °C, four phases are again observed,  $\gamma$ ,  $\gamma'$  and both D0<sub>19</sub> and B2; while after 4000 h the amount of  $\gamma'$  is nearly zero. Results at both of these temperatures suggest that  $\gamma'$  is unstable at all temperatures in

the ternary system. A detailed description of phase equilibrium at these temperatures will be the subject of a future report.

### 3.3 Phase Compositions

Table 2 summarizes the composition data collected from the samples annealed at 900 °C for 4000 h. Figure 8 presents the Co-Al-W 900 °C isothermal section of the phase diagram calculated using the assessment available in the TCNI6 database<sup>[29]</sup> after suspending the  $\gamma'$  to yield a three-phase equilibrium between  $\gamma$ , D0<sub>19</sub>, and B2 (Fig. 8a); and that determined experimentally in the present studied. The phase composition data summarized in Table 2 is overlaid on both diagrams. The phase boundaries in the calculated phase diagram are close to the compositions measured by Kobayashi, the only data available when the assessment was performed. The present compositional data for the  $\gamma$  and D0<sub>19</sub> phase are in good agreement with previous measurements, while those for the B2 phase are leaner in Al than the measurements of Kobayashi. The true equilibrium compositions likely lie between the present measurements and those of Kobayashi. Because the  $\gamma'$  phase has been shown in the present work to be slowly dissolving at 900 °C, the compositions measured here (and in Ref 4, 5) do not represent true equilibrium tie-lines. In principle the compositions of the  $\gamma$ , B2 and D0<sub>19</sub> phases must be all slightly supersaturated compared to what would exist once the  $\gamma'$  phase has dissolved. The measured Al and W levels in  $\gamma$  are likely higher than would exist in  $\gamma$  once the true three-phase  $\gamma + B2 + D0_{19}$  structure equilibrates. Similarly the measured Al level is higher and the W level is lower in the D0<sub>19</sub> phase; and the measured Al and W levels are lower in the B2 phase than would exist in these phase equilibrium has been reached. Thus one-sided error bars could be placed on the measured compositions of the  $\gamma$ , B2 and D0<sub>19</sub> phases. However the phase compositions of  $\gamma$ , D0<sub>19</sub>, and B2 measured in the present work do not change significantly between the 2000 and 4000 h annealing times, or from 4000 to 8000 h, so this error is likely on the order of a few tenths of a mole fraction in Al and W, well within the reported 95 % confidence interval. For instance, the measured B2 composition after 2000 h is 34.06 ± 1.75 % Al and 2.89 ± 0.80 % W, compared to 34.42 ± 1.33 % Al and 2.96 ± 0.23 % W after 4000 h. Complete compositional analysis could not be performed on the 8000 h annealed samples because two of the five ternary alloys were lost, but the EDS measurements that were taken compared very well with those measured after 4000 h.

The other primary difference between the present phase diagram (as well the calculated one) and that reported by Sato is the inclusion of the ferromagnetic to paramagnetic transition in the  $\gamma$  phase. The composition of  $\gamma$  in the binary L01 alloy annealed for 4000 h at 900 °C is consistent with that of the ferromagnetic phase,<sup>[27]</sup> also confirmed by Sato et al.<sup>[28]</sup> According to the binary Al-Co phase diagram, the ferromagnetic-paramagnetic transition in  $\gamma$  occurs near a

<sup>2</sup>Mention of any commercial product is for completeness and does not constitute an endorsement by NIST.

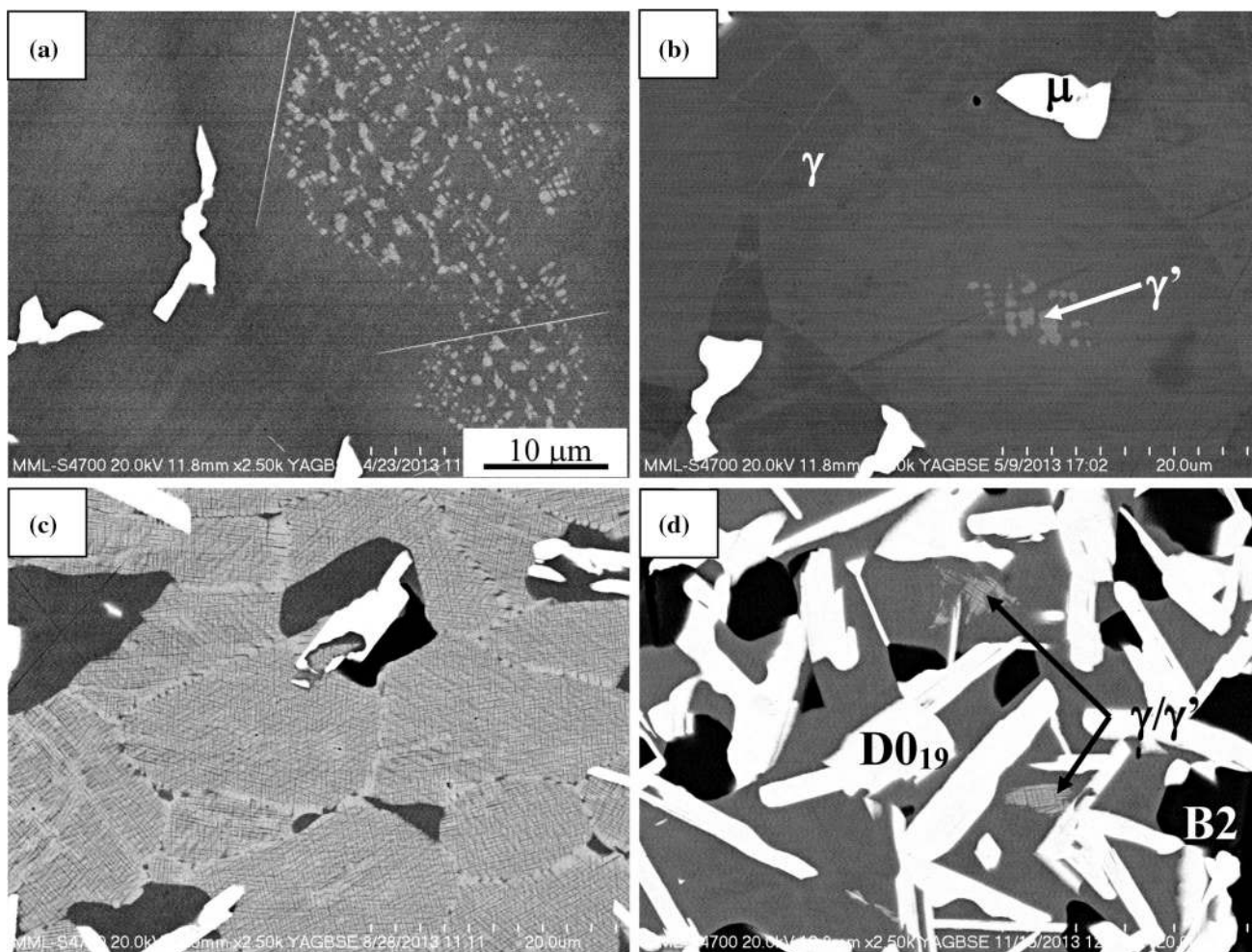


**Fig. 7** Alloy L06 heat treated at 1000 °C for (a) 168 h and (b) 1000 h; and at 850 °C for (c) 2000 h and (d) 4000 h. In (a) and (b) the bright phase is  $\mu$ , not  $D0_{19}$ , the dark gray matrix is  $\gamma$ , and the fine light gray is what remains of the  $\gamma'$ . In (c) and (d) the white is  $D0_{19}$ , black is B2, dark gray is  $\gamma$ , and light gray is  $\gamma'$ . The scale bar in (a) is representative of all images (i.e. the magnifications are the same)

mole fraction of Al of 8 % Al at 900 °C.<sup>[29]</sup> Diffusion couple experiments are presently being conducted by the authors to elucidate on boundaries between the ferromagnetic and paramagnetic phases in this region.

### 3.4 $\gamma'$ Dissolution Kinetics

The reason for the slow dissolution of the  $\gamma'$  phase and the persistence of a four-phase microstructure even after 8000 h of annealing in these alloys is not apparent. Possible explanations include: (1) a quaternary impurity, (2) slow diffusion processes, (3) low driving force for dissolution of  $\gamma'$  or (4) coherent equilibrium effects. Careful examination of EDS spectra from the samples indicates the absence of any other component in the alloys. The detection limit is likely to be a mass fraction of about 0.1 %. Analysis of possible C and O contamination also reveal concentration levels of less than a mass fraction of these elements of 0.1 %.

While W diffusion in these alloys will be significantly slower than Al, it is unlikely the source for the slow

dissolution of the  $\gamma'$  phase. Table 3 lists the available tracer diffusion coefficients in each of the present phases,<sup>[30–35]</sup> while Table 4 lists the calculated W tracer diffusivities at 900 °C for each alloy composition predicted using the assessments published by Cui.<sup>[32,33]</sup> In the matrix,  $\gamma$  phase, the W diffusivity is an order of magnitude slower than the Al diffusivity; however, the estimated diffusion distance at 900 °C after 4000 h is 10  $\mu\text{m}$ . Although there are no measurements of the diffusivity of W in the Co-Al based  $\gamma'$  phase, based on the diffusivity measurements in the Ni-based system the W diffusivity in the  $\gamma'$  Co-Al based alloys is expected to be within 50 % of the diffusivity in the  $\gamma$  phase and have diffusion distance at 900 °C after 4000 h of approximately 7  $\mu\text{m}$ . Nakamura<sup>[34]</sup> measured the self-diffusivity of Co in the CoAl-B2 phase and reported that the diffusivity of Co in the B2 phases is approximately 2 orders of magnitude slower than that in the  $\gamma$  phase. Assuming the W diffusivity in the B2 phase is similar or slower than the Co, the estimated diffusion distance in a B2 phase after 4000 h at 900 °C is approximately 1  $\mu\text{m}$ .

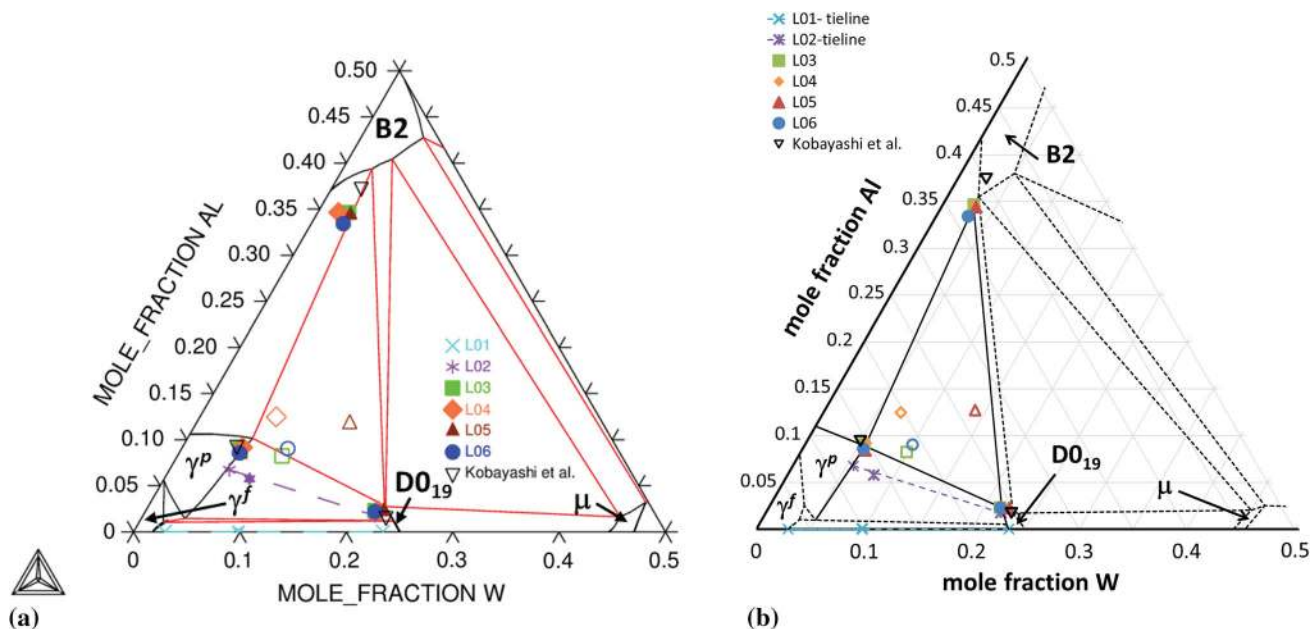


**Fig. 8** (a) The 900 °C isothermal section of the Co-rich Co-Al-W phase diagram calculated using the TCNI6 database, in which the  $\gamma$  has been suspended, and (b) the proposed 900 °C isothermal section determined in the present study. The experimental data collected in the present study and those reported by Kobayashi are shown in both. Open symbols are alloy compositions while filled shapes are phase compositions determined in the present study (L01 and L02 alloy compositions are bold, while phase compositions are not bold).  $\gamma^f$  indicates ferromagnetic  $\gamma$ , while  $\gamma^p$  indicates paramagnetic  $\gamma$

**Table 3** Available tracer diffusivity data for the Co-Al-W system and the calculated diffusion distance after 4000 h at 900 °C

Tracer diffusivity	$D_0$ , $m^2/s$	$Q$ , kJ/mol	$D_0$ , $m^2/s$ at 900 °C	Diffusion distance, $\mu m$ , after 4000 h	Reference
Co in Co ( $\gamma$ )	$2.35 \times 10^{-5}$	281	$6.84 \times 10^{-18}$	10	[30]
Al in Co ( $\gamma$ )	$3.51 \times 10^{-5}$	275	$1.99 \times 10^{-17}$	16	[32]
W in Co ( $\gamma$ )	$3.51 \times 10^{-5}$	282	$9.71 \times 10^{-18}$	12	[31]
Co in CoAl-B2	$4.24 \times 10^{-2}$	416	$1.26 \times 10^{-20}$	0.5	[34]
Co in $\mu$	$1.00 \times 10^{-4}$	243	$1.51 \times 10^{-15}$	145	[35]

**Table 4** Tracer diffusivity of W at 900 °C in each alloy calculated from Ref 32,33, and the resulting diffusion distance after 4000 h

Alloy	Tracer diffusivity of W, $m^2/s$	Diffusion distance, $\mu m$ , after 4000 h
L01	$1.15 \times 10^{-18}$	4.1
L02	$1.98 \times 10^{-18}$	5.3
L03	$1.33 \times 10^{-18}$	4.4
L04	$2.03 \times 10^{-18}$	5.4
L05	$8.79 \times 10^{-18}$	11.2
L06	$1.38 \times 10^{-18}$	4.5

Initial interdiffusion measurements report by Ravi and Paul<sup>[35]</sup> suggest that diffusivity in the  $\mu$  phase is 2 orders magnitude faster than in  $\gamma$  phase. Thus, after 4000 h, and ultimately 8000 h, at 900 °C there should be adequate diffusion to reach equilibrium.

The assumption that the slow dissolution of the  $\gamma'$  phase is not diffusion controlled is also supported by work in the binary Co-W alloy system. Under the same conditions, a melt-spun binary Co-W alloy, which has an initial FCC ( $\gamma$ ) microstructure, forms an equilibrium  $\gamma + D0_{19}$  structure without difficulty after 168 h at 900 °C. It is noted that presently the experimental information on the diffusivity in the Co-W  $D0_{19}$  phase is limited but is thought to be similar to the diffusivity in the related  $L1_2$  structure and to follow “Cu<sub>3</sub>Au” which states that the diffusivity of the minority species is significantly slower than majority species.<sup>[36]</sup> Thus the W diffusivity is expected to be at least an order of magnitude slower than Co in the  $D0_{19}$  structure. Previous studies on the discontinuous precipitation of the Co-W  $D0_{19}$  phase from the  $\gamma$  phase at 900 °C<sup>[37]</sup> indicate that the diffusivity is sufficient that equilibrium should be achieved after 4000 or 8000 h. In addition, preliminary measurements have been conducted by the present authors on diffusion couples in the single phase  $\gamma$  region of the Co-Al-

W system. Diffusion couple microprobe measurements in the  $\gamma$  phase show diffusion distances of approximately 5 and 15  $\mu\text{m}$  for W and Al respectively after 100 h annealing at 900 °C. Comparison of these diffusion distances with the distance between phases seen in Fig. 3 suggests that despite the slow diffusion in the B2 and possibly the  $\text{D0}_{19}$  phases this is not a likely cause for the slow dissolution of the  $\gamma'$  phase.

Another possibility is that there may be a low driving force for the dissolution of  $\gamma'$ . It has been shown that small additions of alloying elements to Co-Al-W alloys can stabilize the  $\gamma'$  phase.<sup>[21–25]</sup> Recent DFT calculations also suggest the energy of the ternary  $\text{Co}_3(\text{Al,W})$   $\text{L1}_2$  intermetallic may lie only a few meV (or  $<1$  kJ/mol) above the convex hull representing equilibrium  $\gamma + \text{B2} + \text{D0}_{19}$ ,<sup>[38]</sup> indicating the driving force for  $\gamma'$  dissolution is likely quite low. This low driving force would be reflected in the microstructural evolution by the existence of very small levels of supersaturation within the phases to drive the diffusion processes required for  $\gamma'$  dissolution. The preliminary results of annealing at 850 °C, where the  $\gamma'$  phase is observed to nearly completely disappear after 4000 h, seem to support this hypothesis; i.e. the driving force for dissolution of  $\gamma'$  is greater at this lower temperature while diffusion remains rapid enough for the alloy to transform. Detailed examination of the microstructure shows contact between all pairs of phases in the four phase mixture, so that existence of a diffusion barrier effect is not likely.

Coherency effects are another possibility. There is considerable evidence for alloys L03 and L04 (see Fig. 3) that fine coherent microstructure of  $\gamma + \gamma'$  persists as a microconstituent of the overall four phase structure for long annealing times. This microstructure remains fine despite the formation and coarsening of the B2 and  $\text{D0}_{19}$  phases. Theoretical analysis of the effects of coherency strain and the elastic contribution to the free energy are known to cause violations of the simple phase rule generally applied to alloy systems.<sup>[39]</sup> Coarse particles of  $\gamma'$  are found in the microstructures of Fig. 3 and 4, coexisting with the fine coherent  $\gamma + \gamma'$  structures. These large particles also appear to be slowly dissolving. Coherency effects combined with a small driving force for  $\gamma'$  dissolution may provide an explanation for its persistence in this ternary alloy system.

## 4. Summary and Conclusions

The approach toward phase equilibrium in the Co-rich portion of the Co-Al-W system was investigated in six melt-spun ribbon compositions. Four of the six as-spun ribbons were a single phase FCC solid solution; while the as-spun microstructure of the 12.5Al-7.5W and 12Al-15W compositions consisted of a primary FCC matrix with 100 nm scale B2 and  $\text{B2} + \mu$  precipitates, respectively. These precipitates were observed to dissolve after 1000 h at 900 °C, and the melt-spun material proved to be a suitably uniform starting material for studying microstructural evolution and approach to equilibria.

The  $\text{L1}_2$ - $\gamma'$  phase was determined to be unstable in the ternary system at 900 °C. This was apparent from the formation of all three equilibrium phases,  $\gamma$ ,  $\text{D0}_{19}$ , and B2 in addition to  $\gamma'$  in alloys selected to be with three-phase regions containing  $\gamma'$  and two of the other three phases; and from the observed decrease in  $\gamma'$  volume fraction with increasing annealing time, accompanied by a corresponding increase in  $\text{D0}_{19}$  or B2, depending on the initial alloy composition. Additionally, heat treatments at 850 and 1000 °C suggested that  $\gamma'$  is most likely a nonequilibrium phase at all temperatures. The phase fraction and compositional data collected in the present study differed slightly from that published by Kobayashi et al.

The precise reasons for the apparent slow dissolution of  $\gamma'$  were unclear. Quaternary element contamination was ruled out. Diffusion in the FCC- $\gamma$  phase was also found to be an unlikely contributor. However, diffusion in the remaining phases, as well as low driving forces for dissolution and coherency effects may all play a role in the slow approach toward equilibrium. Additional investigation is required to determine the exact mechanism involved.

Finally, the phase fraction and compositional measurements, although not true equilibrium values, were very near the equilibrium values, and will provide essential data required for developing an improved understanding of the thermodynamics in ternary Co-Al-W. A new 900 °C isothermal section was presented using the data collected in this study.

## Acknowledgments

EAL would like to thank Dr. William J. Boettinger for the insightful discussions of the results and their interpretation.

## Note Added in Proof

A new paper was accepted for publication in JPED and became available online during the review process for this manuscript. This paper is relevant to the present work. The paper is: J. Zhu, M.S. Titus, T.M. Pollock, “Experimental Investigation and Thermodynamic modeling of the Co-Rich Region in the Co-Al-Ni-W Quaternary System,” JPED, doi: [10.1007/s11669-014-0327-5](https://doi.org/10.1007/s11669-014-0327-5).

## References

1. J. Sato, T. Omori, K. Oikawa, I. Ohnuma, R. Kainuma, and K. Ishida, Cobalt-Based High-Temperature Alloys, *Science*, 2006, **312**, p 90-91
2. T.M. Pollock, J. Dibbern, M. Tsunekane, J. Zhu, and A. Suzuki, New Co-Based g-g' High-Temperature Alloys, *JOM*, 2010, **62**, p 58-63
3. G. Dmitrieva, V. Vasilenko, and I. Melnik, Al-Co-W Fusion Diagram in the Co-CoAl-W Part, *Chem. Met. Alloys*, 2008, **1**, p 338-342

4. S. Kobayashi, Y. Tsukamoto, T. Takasugi, H. Chinen, T. Omori, K. Ishida, and S. Zaeferrer, Determination of Phase Equilibria in the Co-Rich Co-Al-W Ternary System with a Diffusion-Couple Technique, *Intermetallics*, 2009, **17**, p 1085-1089
5. Y. Tsukamoto, S. Kobayashi, and T. Takasugi, The Stability of  $\gamma'$ -Co<sub>3</sub>(Al, W) Phase in Co-Al-W Ternary System, *Mater. Sci. Forum*, 2010, **654-656**, p 448-451
6. F. Xue, M. Wang, and Q. Feng, Phase Equilibria in Co-rich Co-Al-W alloys at 1300 °C and 900 °C, *Mater. Sci. Forum*, 2011, **686**, p 388-391
7. Y.F. Cui, X. Zhang, G.L. Xu, W.J. Zhu, H.S. Liu, and Z.P. Jin, Thermodynamic Assessment of Co-Al-W System and Solidification of Co-Enriched Ternary Alloys, *J. Mater. Sci.*, 2011, **46**, p 2611-2621
8. *TCNI6 Ni-Based Superalloy Database*, Thermo-Calc Software AB, Stockholm, Sweden, 2013
9. *PanCobalt Thermodynamic*, Computherm LLC, Madison, WI, USA, 2014
10. S. Miura, K. Ohkubo, and T. Mohri, Mechanical Properties of Co-Based L12 Intermetallic Compound Co<sub>3</sub>(Al, W), *Mater. Trans.*, 2007, **48**, p 2403
11. A. Suzuki, G.C. DeNolf, and T.M. Pollock, Flow Stress Anomalies in  $\gamma/\gamma'$  Two-Phase Co-Al-W-Base Alloys, *Scripta Mater.*, 2007, **56**, p 385-388
12. A. Suzuki and T.M. Pollock, High-Temperature Strength and Deformation of  $\gamma/\gamma'$  Two-Phase Co-Al-W-Base Alloys, *Acta Mater.*, 2008, **56**, p 1288-1297
13. A. Bauer, S. Neumeier, F. Pyczak, and M. Göken, Microstructure and Creep Strength of Different  $\gamma/\gamma'$ -Strengthened Co-Base Superalloy Variants, *Scripta Mater.*, 2010, **63**, p 1197-1200
14. H. Inui, T. Oohashi, N.L. Okamoto, K. Kishida, and K. Tanaka, Mechanical Properties of the Ternary L12 Compound Co<sub>3</sub>(Al, W) in Single and Polycrystalline Forms, *Adv. Mater. Res.*, 2011, **287**, p 1-6
15. M. Titus, A. Suzuki, and T.M. Pollock, Creep and Directional Coarsening in Single Crystals of New  $\gamma-\gamma'$  Cobalt-Base Alloy, *Scripta Mater.*, 2012, **66**, p 574-577
16. A. Bauer, S. Neumeier, F. Pyczak, R.F. Singer, and M. Göken, Creep Properties of Different  $\gamma'$ -Strengthened Co-Based Superalloys, *Mater. Sci. Eng. A*, 2012, **550**, p 333-341
17. F. Pyczak, A. Bauer, M. Göken, S. Neumeier, U. Lorenz, M. Oehring, N. Schell, A. Schreyer, A. Stark, and F. Symanzik, Plastic Deformation Mechanisms in a Crept L12 Hardened Co-Base Superalloy, *Mater. Sci. Eng. A*, 2013, **571**, p 13-18
18. S. Meher, H.-Y. Yan, S. Nag, D. Dye, and R. Banerjee, Solute Partitioning and Site Preference in  $\gamma/\gamma'$  Cobalt-Base Alloys, *Scripta Mater.*, 2012, **67**, p 850-853
19. P.J. Bocchini, E.A. Lass, K.-W. Moon, M.E. Williams, C.E. Campbell, U.R. Kattner, D.C. Dunand, and D.N. Seidman, Atom-Probe Tomographic Study of  $\gamma/\gamma'$  Interfaces and Compositions in an Aged Co-Al-W Superalloys, *Scripta Mater.*, 2013, **68**, p 563-566
20. S. Meher, S. Nag, J. Tiley, A. Goel, and R. Banerjee, Coarsening Kinetics of  $\gamma'$  Precipitates in Cobalt-Base Alloys, *Acta Mater.*, 2013, **61**, p 4266-4276
21. K. Shinagawa, T. Omori, J. Sato, K. Oikawa, I. Ohnuma, R. Kainuma, and K. Ishida, Phase Equilibria and Microstructure on  $\gamma'$  Phase in Co-Ni-Al-W System, *Mater. Trans.*, 2008, **49**, p 1474-1479
22. M. Ooshima, K. Tanaka, N.L. Okamoto, K. Kishida, and H. Inui, Effects of Quaternary Alloying Elements on the  $\gamma'$  Solvus Temperature of Co-Al-W Based Alloys with fcc/L1<sub>2</sub> Two-Phase Microstructures, *J. Alloys Compds.*, 2010, **508**, p 71-78
23. S. Kobayashi, Y. Tsukamoto, and T. Takasugi, Phase Equilibria in the Co-Rich Co-Al-W-Ti Quaternary System, *Intermetallics*, 2011, **19**, p 1908-1912
24. S. Kobayashi, Y. Tsukamoto, and T. Takasugi, The Effects of Alloying Elements (Ta, Hf) on the Thermodynamic Stability of  $\gamma'$ -Co<sub>3</sub>(Al, W) Phase, *Intermetallics*, 2012, **31**, p 94-98
25. T. Omori, K. Oikawa, J. Sato, I. Ohnuma, U.R. Kattner, R. Kainuma, and K. Ishida, Partition Behavior of Alloying Elements and Phase Transformation Temperatures in Co-Al-W-Base Quaternary Systems, *Intermetallics*, 2013, **32**, p 274-283
26. B.N. Taylor, C.E. Kuyatt, *Guidelines for Evaluating and Expressing the Uncertainty of NIST Measurement Results*, NIST Technical Note 1297, 1994 Edition, United States Department of Commerce, Technology Administration, National Institute of Standards and Technology
27. A. Markström, B. Sundman, and K. Frisk, A Revised Thermodynamic Description of the Co-W-C System, *J. Phase Equil. Diff.*, 2005, **26**, p 152-160
28. J. Sato, K. Oikawa, R. Kainuma, and K. Ishida, Experimental Verification of Magnetically Induced Phase Separation in  $\alpha$ Co Phase and Thermodynamic Calculations of Phase Equilibria in the Co-W System, *Mater. Trans.*, 2005, **46**, p 1199-1207
29. A.J. McAlister, Al-Co (Aluminum-Cobalt), *Binary Alloy Phase Diagrams*, 2nd ed., T.B. Massalski, Ed., vol. 1, 1990, p 136-138
30. G. Neumann, V. Tölle, and C. Tuijn, Application of the Modified Electrostatic Model to the Impurity Diffusion in Cobalt, *Phys. B*, 2001, **304**, p 298-303
31. J. Ruzicková, B. Million, and J. Kucera, Heterodiffusion of W-185 in gamma-Fe, Co, and Ni, *Kovové Mater.*, 1981, **19**, p 3
32. Y.-W. Cui, B. Tang, R. Kato, R. Kainuma, and K. Ishida, Interdiffusion and Atomic Mobility for Face-Centered-Cubic Co-Al Alloys, *Metall. Mater. Trans. A*, 2011, **42A**, p 2542-2546
33. Y.-W. Cui, G. Xu, R. Kato, X.-G. Lu, R. Kainuma, and K. Ishida, Interdiffusion and Atomic Mobility for Face-Centered Cubic (FCC) Co-W Alloys, *Metall. Mater. Trans. A*, 2013, **44A**, p 1621-1625
34. R. Nakamura and Y. Iijima, Self-Diffusion of Cobalt in B2 Type Intermetallic Compound CoAl, *Intermetallics*, 2005, **13**, p 163-167
35. R. Ravi and A. Paul, Interdiffusion Study on Co(W) Solid Solution and Topological Close-Packed  $\mu$  Phase in Co-W System, *Intermetallics*, 2011, **19**, p 426-428
36. H. Mehrer, Diffusion in Intermetallics, *Mater. Trans. JIM*, 1996, **37**, p 1259-1280
37. P.A. Carvalho, P.M. Bronsveld, B.J. Kooi, and JThM De Hosson, On the fcc  $\rightarrow$  D019 Transformation in Co-W Alloys, *Acta Mater.*, 2002, **50**, p 4511-4526
38. J.E. Saal and C. Wolverton, Thermodynamic Stability of Co-Al-W L1<sub>2</sub>  $\gamma'$ , *Acta Mater.*, 2013, **61**, p 2330-2338
39. W.C. Johnson, On the Inapplicability of Gibbs Phase Rule to Coherent Solids, *Metall. Trans. A*, 1987, **18A**, p 1093-1097